Contributions to Mineralogy and Petrology (2020) 175:62
https://doi.org/10.1007/s00410-020-01695-z

ORIGINAL PAPER

# Fe–Mg and Fe–Mn interdiffusion in ilmenite with implications for geospeedometry using oxides

**Kelsey B. Prissel[1] · Michael J. Krawczynski[1] · James A. Van Orman[2]**

Received: 12 November 2019 / Accepted: 19 May 2020


## Abstract

The Fe–Mg and Fe–Mn interdiffusion coefficients for ilmenite have been determined as a function of temperature and crystallographic orientation. Diffusion annealing experiments were conducted at 1.5 GPa between 800 and 1100 °C. For Fe–Mg interdiffusion, each diffusion couple consisted of an ilmenite polycrystal and an oriented single crystal of geikielite. The activation energy ($Q$) and pre-exponential factor ($D_0$) for Fe–Mg diffusion in the ilmenite polycrystal were found to be $Q = 188 \pm 15$ kJ mol$^{-1}$ and $\log D_0 = -6.0 \pm 0.6$ m$^2$ s$^{-1}$. For the geikielite single crystal, Fe–Mg interdiffusion has $Q = 220 \pm 16$ kJ mol$^{-1}$ and $\log D_0 = -4.6 \pm 0.7$ m$^2$ s$^{-1}$. Our results indicate that crystallographic orientation did not significantly affect diffusion rates. For Fe–Mn interdiffusion, each diffusion couple consisted of one ilmenite polycrystal and one Mn-bearing ilmenite polycrystal. For Fe–Mn interdiffusion, $Q = 264 \pm 30$ kJ mol$^{-1}$ and $\log D_0 = -2.9 \pm 1.3$ m$^2$ s$^{-1}$ in the ilmenite. We did not find a significant concentration dependence for the Fe–Mg and Fe–Mn interdiffusion coefficients. In comparing our experimental results for cation diffusion in ilmenite with those previously reported for hematite, we have determined that cation diffusion is faster in ilmenite than in hematite at temperatures <1100 °C. At oxygen fugacities near the wüstite–magnetite buffer, Fe and Mn diffusion rates are similar for ilmenite and titanomagnetite. We apply these experimentally determined cation diffusion rates to disequilibrium observed in ilmenites from natural volcanic samples to estimate the time between perturbation and eruption for the Bishop Tuff, Fish Canyon Tuff, Mt. Unzen, Mt. St. Helens, and kimberlites. When integrated with natural observations of chemically zoned ilmenite and constraints on pre-eruptive temperature and grain size, our experimentally determined diffusivities for ilmenite can be used to estimate a minimum time between magmatic perturbation and eruption on the timescale of hours to months.

**Keywords** Ilmenite · Diffusion · Oxide geothermometry · Kimberlites

## Introduction

Ilmenite is an important and widespread accessory phase present in a variety of igneous rocks ranging in composition from silica-undersaturated kimberlites to high-silica rhyolites. Though rarely an abundant mineral in its host rocks, the near ubiquitous presence of ilmenite and the sensitivity of ilmenite composition to temperature and oxygen fugacity make it an important mineral for interpreting the thermal and physical conditions of magmas. Ilmenite is a rhombohedral oxide with the end-member composition $Fe^{2+}TiO_3$. Generally, "ilmenite" refers to the layered octahedral atomic structure with formula $A^{2+}B^{4+}O_3$, where $A^{2+}$ and $B^{4+}$ represent charged cations (e.g. $Fe^{2+}$, $Mg^{2+}$, $Mn^{2+}$, $Ti^{4+}$). The terms "ilmenite" and "hemo-ilmenite" have also been used to refer to compositions represented

Communicated by Mark S Ghiorso.

**Electronic supplementary material** The online version of this article (https://doi.org/10.1007/s00410-020-01695-z) contains supplementary material, which is available to authorized users.

✉ Kelsey B. Prissel
k.b.williams@wustl.edu

[1] Department of Earth and Planetary Sciences, Washington University in St. Louis, Campus Box 1169, 1 Brookings Drive, St. Louis, MO 63130-4899, USA

[2] Department of Earth, Environmental, and Planetary Sciences, Case Western Reserve University, 10900 Euclid Avenue, Cleveland, OH 44106, USA

Published online: 10 June 2020

by the solid solution between ilmenite, $Fe^{2+}TiO_3$, and the isostructural mineral hematite, ($Fe_2^{3+}O_3$).

Coexisting ilmenite and titanomagnetite (solid solutions of magnetite and ulvöspinel) mineral pairs have been used extensively to infer the pre-eruptive conditions, namely temperature and oxygen fugacity, of magmas beneath volcanic complexes (e.g. Buddington and Lindsley 1964; Pownceby et al. 1987; Bishop 1980; Bacon and Hirschmann 1988; Ghiorso and Evans 2008). However, these methods are based on equilibrium between ilmenite and titanomagnetite, and thus any disequilibrium between the two minerals precludes the use of the oxide compositions in geothermometers or oxybarometers. In practice, the Mg/Mn ratios of coexisting ilmenites and titanomagnetites are used to identify disequilibrium oxide pairs in rapidly cooled volcanic rocks (e.g. Bacon and Hirschmann 1988). Evidence for non-equilibrium in ilmenite also exists as chemical zoning, including but not limited to volcanic rocks from Mt. St. Helens (Rutherford and Devine III 2008), Mt. Unzen (Venezky and Rutherford 1999), kimberlites (Pasteris 1981; Mitchell 1986; Schulze et al. 1995), and the Moon (Taylor et al. 1975).

The preservation of disequilibrium oxide compositions and chemical zoning in ilmenite yield insight into the dynamic processes occurring in ilmenite-bearing volcanic systems such as melting, heating, mixing, ascent, and eruption. Quantifying the rates and timescales of magmatic processes is important to understanding magma transport, differentiation, and mixing prior to eruption. The rates of volcanic processes are often estimated using experimentally determined diffusion coefficients in diffusion models to match concentration gradients observed in minerals, particularly for the silicate minerals olivine, feldspar, pyroxene, and quartz (e.g. Costa et al. 2008; Zhang and Cherniak 2010; Till et al. 2015; Shea et al. 2015). Diffusion studies have also been conducted on many oxide minerals, including periclase, spinel, titanomagnetite, and rutile (Van Orman and Crispin 2010, and references therein). In particular, Fe–Mg interdiffusion rates have been well characterized experimentally for a diversity of major rock-forming minerals including olivine (Chakraborty 1997), pyroxene (Müller et al. 2013), and spinel (Vogt et al. 2015). Despite the common occurrence of ilmenite and its well-studied equilibrium compositions, there has yet to be a quantitative study of the diffusivity of cations ($Fe^{2+}$, $Fe^{3+}$, $Mg^{2+}$, $Mn^{2+}$, $Ti^{4+}$) in the ilmenite mineral structure.

Here, we present the first experimentally determined Fe–Mg and Fe–Mn interdiffusivities for ilmenite. With the use of the cation interdiffusion coefficients determined in this study, the compositional profiles preserved in ilmenites can constrain the rates of rapid volcanic processes. We apply these new data to Mg/Mn disequilibrium observed in natural coexisting oxide pairs (ilmenite and titanomagnetite), and to Mg zoning in ilmenite megacrysts found in kimberlites.

## Experimental, analytical, and numerical methods

### Experimental approach

Diffusion experiments were conducted in a piston cylinder apparatus at 1.5 GPa pressure to investigate the diffusivity of $Fe^{2+}$, $Mg^{2+}$, and $Mn^{2+}$ in ilmenite solid solutions between 800 and 1100 °C. Synthetic polycrystalline ilmenite was juxtaposed against either an oriented, synthetic geikielite ($MgTiO_3$) crystal or a synthetic polycrystalline Mn-bearing ilmenite in a "diffusion-couple" geometry.

#### Starting material synthesis and purity

Polycrystalline ilmenites were synthesized by mixing high-purity reagent-grade oxides (FeO, MnO, and $TiO_2$) in stoichiometric proportion (ilmenite, $FeTiO_3$, and Mn-bearing ilmenite, $Fe_{0.95}Mn_{0.05}TiO_3$). Starting materials were produced using two sources of iron: (1) all FeO or (2) a mixture of Fe-metal and $Fe_2O_3$ (1:1 molar ratio). The iron, manganese, and titanium oxides were mixed under isopropanol in a silicon-nitride ball mill for 3 h. For mixes with Fe-metal (#001, #007, and #019), the Fe-metal was added after ball mill mixing, and the mixture was ground by hand in an agate mortar until the isopropanol evaporated. The ground starting material was then packed into a graphite capsule (approximately 7 mm depth) and sintered in a piston cylinder apparatus at either 1140 °C and 1.5 GPa or 1165 °C and 1.75 GPa for approximately 3 days (Online Resource 2). The graphite capsule limits the oxygen fugacity of the experiment to below the graphite–COH buffer producing $Fe^{2+}TiO_3$ with minimal hematite solution (Ulmer and Luth 1991; Médard et al. 2008). Using the empirical relationship determined in Ulmer and Luth (1991) for high-pressure experiments conducted using graphite capsules, we have calculated the upper limit of the oxygen fugacity for our synthesis and diffusion annealing experiments. Relative to the quartz–fayalite–magnetite (QFM) buffer, the upper limit on the oxygen fugacity of the synthesis experiments is QFM − 1.2. The upper limit on the oxygen fugacity of our diffusion annealing experiments ranges from QFM − 0.4 at 800 °C to QFM − 1.3 at 1200 °C. However, the presence of Fe metal in the ilmenite polycrystals after the synthesis and diffusion annealing experiments indicates the oxygen fugacity conditions of the graphite capsules were more reducing than these estimated upper limits. Sintered polycrystalline ilmenite cylinders

were cut into thin, circular wafers, mounted in epoxy, and polished. Geikielite ($MgTiO_3$) single crystals were provided by Jeremy N. Mitchell of Los Alamos National Laboratory, and are described in Mitchell et al. (1998).

The synthetic ilmenite wafers and geikielite were examined for homogeneity by electron microscopy. The synthetic polycrystalline ilmenite aggregates were composed of subhedral crystals 20–200 µm in diameter. Ilmenites synthesized from starting materials containing Fe-metal (mixes #001, #007, and #019) had iron metal present as an accessory phase. Synthetic Mn-bearing ilmenite wafers included minor amounts of ulvöspinel ($FeTi_2O_4$). Thin needles (< 2 µm thickness, average 20 µm length) of rutile ($TiO_2$) were present in the synthetic geikielite single crystals both before and after the experiments (Fig. 3).

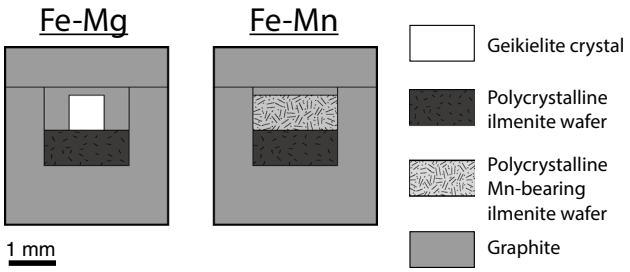


**Fig. 1** Schematic diagram of the experimental diffusion couple geometry. Each ilmenite polycrystal was polished then loaded into a graphite capsule such that the polished face would come into contact with the other half of the diffusion couple (Mn-bearing ilmenite polycrystal or geikielite single crystal). Geikielite single crystals were oriented such that the *c*-axis was either perpendicular or parallel to the diffusion interface. Graphite powder was used to fill the void space of each capsule and prevent the diffusion couple halves from separating during sample assembly

### Diffusion annealing experiments

Diffusion-annealing experiments were conducted in a 0.5" piston cylinder apparatus (Boyd and England 1960) in the experimental geochemistry laboratory at Washington University in St. Louis. The polished face of an oriented synthetic geikielite cube was juxtaposed against the polished face of a synthetic polycrystalline ilmenite wafer. The geikielite cubes were prepared by cutting a single crystal of synthetic geikielite into 1-mm-thick wafers, then slicing each wafer into approximately 1-mm edge-length cubes. The cubes were polished either perpendicular or parallel to the *c*-axis. Orientation of each cube was confirmed using crossed-polarized reflected light. In each Fe–Mg interdiffusion experiment, the geikielite cube was oriented to explore the effect of crystallographic orientation on diffusion. Because the crystals have rhombohedral symmetry, two diffusion directions were investigated: one in which diffusion occurred perpendicular to the *c*-axis (⊥c), and one in which diffusion occurred parallel to the *c*-axis (‖c). To investigate Fe–Mn interdiffusion, two synthetic polycrystalline ilmenite wafers, one containing Mn and one initially Mn-free, were juxtaposed so that the polished faces of each wafer were in contact. For each diffusion annealing experiment, the diffusion couple was contained within a graphite capsule and the void spaces of the capsule were filled with graphite powder (Fig. 1).

Piston cylinder experiments were performed between 800 and 1100 °C at 1.5 GPa (Table 1). Temperature was increased to the desired sample temperature at a rate of 100 °C per minute. Sample temperature was controlled to within 1–2 °C of the reported temperature throughout the experiment, as monitored by a Eurotherm PID temperature controller. The difference between the Type-C (W-5%Re/W-26%Re) thermocouple reading and sample temperature for the experimental assembly was calibrated using the spinel reaction-progress thermometer (Watson et al. 2002). Experimental pressure was maintained during the experiment by an automatic pressure control system using the hot piston-in technique (Johannes et al. 1971). Experiments were quenched rapidly (approximately 70 °C per second) by turning off the power to the apparatus. Experimental run duration was defined as the time between reaching the experimental target temperature and quench. Each experimental capsule was mounted in epoxy and cut perpendicular to the diffusion interface. Then half of the capsule was mounted in epoxy and the cut face was polished in preparation for electron microprobe analysis.

## Analytical methods

Experimental run products were analyzed using a JEOL 8200 electron microprobe at Washington University in St. Louis. Electron microprobe analyses were obtained perpendicularly across the diffusion interface for each experiment. Each quantitative analysis used a 15 kV accelerating potential, 25 nA beam current, and 45 s on-peak counting time. Standardization was performed with a beam diameter of 20 µm on natural and synthetic glass and mineral samples (synthetic Taylor MgO, synthetic Taylor spinel, synthetic Shankland forsterite, synthetic Mn-olivine, synthetic $TiO_2$, natural Elba Hematite, natural Ilmen Mountains ilmenite NMNH 96189, and natural Kakanui hornblende NMNH 143965). Minimum detection limits were 100–300 ppm ($3\sigma$) for all elements. Each linear analytical traverse was positioned to avoid any accessory phases or large cracks in the diffusion couple. Multiple traverses were measured on the experiments in order to assess the consistency of the calculated diffusivities in a single sample. Beam diameter (1–4 µm) was set equal to half of the point spacing on each traverse to avoid point overlap (i.e., 2 µm beam diameter for 4 µm spacing). Compositional data were reduced using Probe for EPMA software (https://www.probe

**Table 1** Experimental run details

| Experiment | Ilmenite[a] | Type | Direction[b] | T (°C) | P (GPa) | Time (s) |
|---|---|---|---|---|---|---|
| **Fe–Mg ⊥c** | | | | | | |
| F032 | D007 | Fe–Mg | ⊥c | 1200 | 1.5 | 3520 |
| MK24 | MK22 | Fe–Mg | ⊥c | 1100 | 1.5 | 20820 |
| F111 | F055 | Fe–Mg | ⊥c | 1100 | 1.5 | 78300 |
| F045 | F043 | Fe–Mg | ⊥c | 1000 | 1.5 | 80440 |
| F110 | F055 | Fe–Mg | ⊥c | 1000 | 1.5 | 260340 |
| F119 | F116 | Fe–Mg | ⊥c | 1000 | 1.5 | 524940 |
| F030 | D009 | Fe–Mg | ⊥c | 900 | 1.5 | 258320 |
| F053 | F049 | Fe–Mg | ⊥c | 800 | 1.5 | 522100 |
| **Fe–Mg ‖c** | | | | | | |
| F018 | F012 | Fe–Mg | ‖c | 1100 | 1.5 | 17940 |
| F019 | F007 | Fe–Mg | ‖c | 1000 | 1.5 | 28680 |
| F117 | F112 | Fe–Mg | ‖c | 1000 | 1.5 | 87060 |
| F033 | D007 | Fe–Mg | ‖c | 900 | 1.5 | 252300 |
| F051 | F044 | Fe–Mg | ‖c | 900 | 1.5 | 261930 |
| F118 | F116 | Fe–Mg | ‖c | 900 | 1.5 | 258840 |
| F086 | F055 | Fe–Mg | ‖c | 800 | 1.5 | 517850 |
| **Fe–Mn** | | | | | | |
| F024 | F022, F023 | Fe–Mn | | 1100 | 1.5 | 15760 |
| F029 | F026, F027 | Fe–Mn | | 1000 | 1.5 | 70390 |
| F031 | D008, D009 | Fe–Mn | | 900 | 1.5 | 252730 |
| F028 | F026, F027 | Fe–Mn | | 800 | 1.5 | 509590 |

[a]Ilmenite column indicates the synthesis experiment(s) for the starting polycrystalline ilmenite(s) in each diffusion couple. Run details for synthesis experiments have been provided in Online Resource 2

[b]Direction describes whether the geikielite single crystal was oriented such that the interdiffusion occurred perpendicular to (⊥c) or parallel to (‖c) the *c*-axis

software.com) and then filtered to exclude analyses where the analytical totals were less than 98.5 wt% or greater than 101.5 wt%, as well as analyses where the cation total for 3 oxygen atoms were less than 1.98 or greater than 2.02 (ideal ilmenite stoichiometry contains 2 cations per 3 oxygen atoms). Two experiments, F045 and F051, have low analytical totals (93–97 wt%), and these are discussed in Sect. 4.3. A detailed discussion of analytical totals is presented in Online Resource 1.

## Numerical analysis of diffusion profiles

Elemental concentration profiles (Fe and Mg or Mn) were used to determine the Fe–Mg or Fe–Mn interdiffusion coefficient for each experiment. Diffusion was modeled as one-dimensional, concentration-independent diffusion in a semi-infinite medium with constant interface concentration (Crank 1975):

$$\frac{C(x,t) - C_{\text{initial}}}{C_{\text{interface}} - C_{\text{initial}}} = erf\frac{x}{2\sqrt{Dt}}, \quad (1)$$

where $D$ is the interdiffusion coefficient ($m^2\ s^{-1}$), $C(x, t)$ is the concentration (mol $m^{-3}$) at position $x$ (m) after the experimental run time $t$ (s), $C_{\text{initial}}$ is the initial concentration on one side of the diffusion couple (e.g., $C_{\text{initial}} = 1$ for mol $MgTiO_3$ in geikielite), and $C_{\text{interface}}$ is the concentration at the diffusion couple interface. This treatment is valid as long as the experimental diffusion profile levels out to the initial concentration in the crystal. In our experiments, the length of the observed concentration profiles on each side of the diffusion interface (< 300 µm) is less than the length of the single geikielite crystal or ilmenite polycrystal (> 500 µm).

To determine the interdiffusion coefficient for each compositional profile, the diffusion profile was linearized by plotting the inverse of the error function

$$erf^{-1}\frac{C_{\text{interface}} - C(x,t)}{C_{\text{interface}} - C_{\text{initial}}} \quad (2)$$

against position ($x$) for each half of the diffusion couple. The values for $C_{\text{interface}}$ and $C_{\text{initial}}$ were determined from the electron microprobe compositional analyses on each experiment. Then fitting a straight line to the linearized compositional profile gave the slope, $(4Dt)^{-1/2}$, from which $D$ was calculated for each half of the diffusion couple (Fig. 2).

The compositions used for the diffusion profile fitting were the measured Fe and Mn atomic percents (Fe

for Fe–Mg interdiffusion, Mn for Fe–Mn interdiffusion), which, unlike using molecular compositions of $FeTiO_3$, avoids any assumption regarding the oxidation state of Fe in each sample. Fits using the molecular compositions, $FeTiO_3$ and $MnTiO_3$, yield similar $D$ values for experiments for which there was no hematite component. Often the two halves of the diffusion couple separated during decompression after the experimental run, resulting in a gap (< 35 µm width) along the diffusion interface (Fig. 3b). Prior to fitting, the $x$ values for the measured diffusion profiles were adjusted by subtracting the gap distance (as measured from back-scattered electron image) so that the compositional profiles measured on each side of the diffusion couple met near the defined diffusion interface, $x = 0$. The position and compositional data for each diffusion profile have been provided in Online Resource 3.

## Results

The interdiffusion coefficients determined in each experiment are reported in Table 2. For each experiment, the reported $D_{Fe-Mg}$ or $D_{Fe-Mn}$ is the average value obtained from multiple profiles across the interface in the diffusion couple and the "uncertainty" is defined by the standard deviation of the results from $n$ traverses multiplied by a Student's $t$ value that corresponds to a two-sided 70% confidence interval for $n - 1$ traverses. For experiments with only one traverse ($n = 1$), we assigned a 10% error as the standard deviation for the weighted linear regression. Some profiles exhibit slight asymmetry with respect to the diffusion interface, suggesting there may be a compositional dependence for the interdiffusion coefficients. However, we were not able to quantify this compositional dependence, and if any compositional dependence exists, it is minor.

Ulvöspinel ($Fe_2TiO_4$) was present as an accessory phase in the polycrystalline sides of the experimental run products, most notably in the Mn-bearing diffusion couples (Fig. 3c). Additionally, the geikielite in experiment F032 contained minor amounts of qandilite ($Mg_2TiO_4$). Qandilite has been noted to occur as an accessory phase in the geikielite starting material (Mitchell et al. 1998). We only observed qandilite in this experiment (F032), and we suspect the presence of qandilite has slightly affected the diffusion in the geikielite single crystal. To obtain interdiffusion coefficients that best represent diffusion in the ilmenite phase, electron microprobe traverses were positioned in regions of the experimental run product that were free of any accessory phases (Fig. 3). Thus, the presence or exsolution of accessory phases during the experiment has little effect on the calculated cation diffusion rates.

### Time series

An isothermal time series of experiments was conducted at 1000 °C to evaluate the reproducibility of the calculated interdiffusion coefficients (Fig. 4). The time series investigated Fe–Mg diffusion with the geikielite crystal oriented such that diffusion was perpendicular to the c-axis. Run durations ranged from 1 to 6 days (Table 2). The interdiffusion coefficients calculated for the ilmenite side of the 1-, 3-, and 6-day experiments are the same within the estimated uncertainty. Further, the interdiffusion coefficient calculated from the geikielite side of the 6-day experiment is within the estimated uncertainty of those calculated from the ilmenite side. The interdiffusion coefficient calculated for the geikielite side of the 1-day experiment is similar to that calculated from the 3-day experiment. Two additional Fe–Mg interdiffusion experiments (MK24 and F111) are included in Fig. 4. These experiments were both conducted at 1100 °C with varied run durations (approximately 6 h and

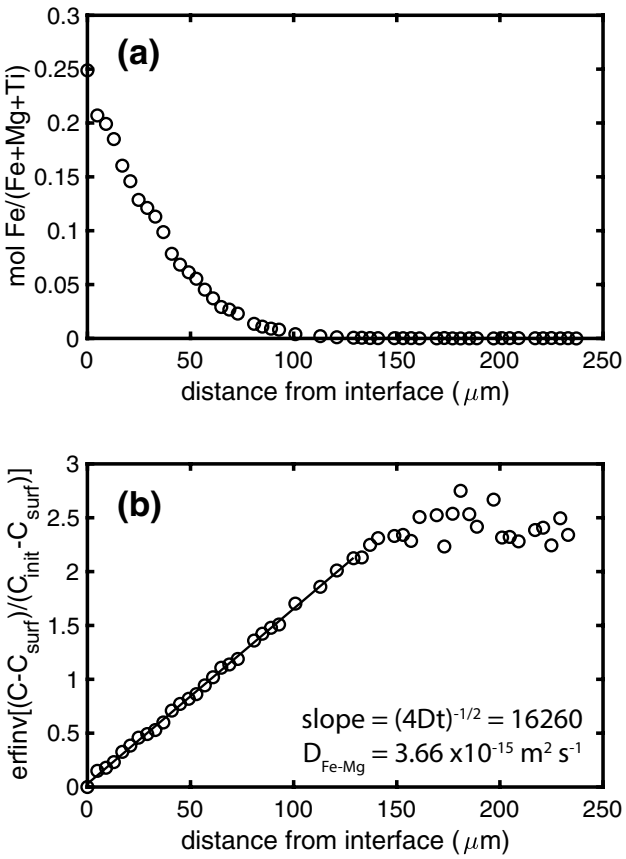


**Fig. 2** **a** Analytical traverse taken in the geikielite single crystal from experiment F030 (analysis line 2). The analyses are plotted as Fe mol fraction (mol Fe/(mol Fe + mol Mg + mol Ti). Analytical uncertainty is smaller than the size of the data symbols. **b** Inverse error function plot of the profile in **a**. The line through the points represents the linear fit from which $D_{Fe-Mg}$ was determined (as described in Sect. 2.3)

**Table 2** Average profile fitting results from *n* analytical traverses for each experiment

| Experiment | T (°C) | polycrystal | | | single crystal | | |
|---|---|---|---|---|---|---|---|
| | | log D ($m^2$ $s^{-1}$) | 1$\sigma$ | n | log D ($m^2$ $s^{-1}$) | 1$\sigma$ | n |
| **Fe–Mg ⊥c** | | | | | | | |
| F032 | 1200 | − 12.6 | 0.2 | 3 | − 13.0 | 0.3 | 3 |
| MK24 | 1100 | − 13.1 | 0.3 | 3 | − 12.6 | 0.2 | 3 |
| F111 | 1100 | − 13.2 | 0.4 | 2 | − 12.9 | 0.3 | 2 |
| F045 | 1000 | − 13.8 | 0.4 | 2 | − 13.5 | 0.3 | 2 |
| F110 | 1000 | − 13.7 | 0.2 | 3 | − 13.5 | 0.2 | 3 |
| F119 | 1000 | − 13.8 | 0.2 | 3 | − 14.0 | 0.2 | 3 |
| F030 | 900 | − 14.6 | – | 1 | − 14.4 | 0.3 | 2 |
| F053 | 800 | − 15.1 | – | 1 | − 15.4 | 0.2 | 3 |
| **Fe–Mg ‖c** | | | | | | | |
| F018 | 1100 | − 12.5 | 0.3 | 2 | − 12.8 | 0.4 | 2 |
| F019 | 1000 | − 13.1 | 0.3 | 2 | − 13.6 | 0.3 | 2 |
| F117 | 1000 | − 13.7 | 0.3 | 3 | n.d. | n.d. | n.d. |
| F033 | 900 | − 14.9 | 0.2 | 4 | − 14.3 | 0.1 | 4 |
| F051 | 900 | − 15.2 | 0.2 | 4 | − 14.2 | 0.1 | 4 |
| F118 | 900 | − 14.0 | 0.2 | 3 | − 14.3 | 0.2 | 3 |
| F086 | 800 | − 14.8 | 0.1 | 3 | − 15.4 | 0.2 | 3 |
| **Fe–Mn** | | | | | | | |
| F024 | 1100 | − 12.8 | 0.7 | 2 | | | |
| F029 | 1000 | − 13.7 | 0.2 | 6 | | | |
| F031 | 900 | − 14.9 | 0.2 | 4 | | | |
| F028 | 800 | − 15.4 | 0.6 | 5 | | | |
| F158 | 800 | − 15.1 | 0.3 | 4 | | | |
| F102 | 800 | − 16.0 | 0.2 | 4 | | | |

*n* = number of profiles used to determined reported average *lnD* value and uncertainty

Reported uncertainty (1$\sigma$) was calculated using the two-sided 70% confidence interval student's *t* multiplier for $n - 1$. For experiments with only one traverse ($n = 1$), we assigned a 10% error as the standard deviation to be used in the weighted linear regression

"n.d." indicates a diffusion coefficient was not determined for this sample

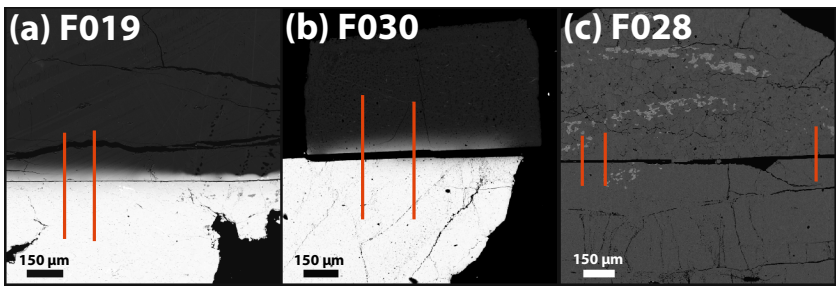


**Fig. 3** Back-scattered electron images for two Fe–Mg interdiffusion experiments (F019, **a** and F030, **b**), and one Fe–Mn interdiffusion experiment (F028, **c**). Each experiment is marked with red lines to indicate the location of the electron microprobe traverses positioned on each sample. For the two Fe–Mg interdiffusion experiments, the dark side of the couple is the geikielite single crystal ($MgTiO_3$) and the bright side of the couple is the ilmenite polycrystal ($FeTiO_3$). **a** Cracks form parallel to the diffusion interface during decompression of the experiment. For profiles that go across decompression cracks, we have adjusted the distance from the interface used in the profile fitting by subtracting the width of the crack for analyses taken on the side of the crack away from the interface. **b** Often, the two sides of the diffusion couple separate during decompression. Before fitting the profiles, we adjust the profile distances by subtracting the width of the gap. The thin bright phases in the geikielite single crystal are rutile ($TiO_2$). **c** The Mn-bearing ilmenite polycrystal is positioned on the top in this image. The bright gray phase present in the both polycrystals, though of greater abundance in the Mn-bearing ilmenite, is ulvöspinel ($Fe_2TiO_4$)

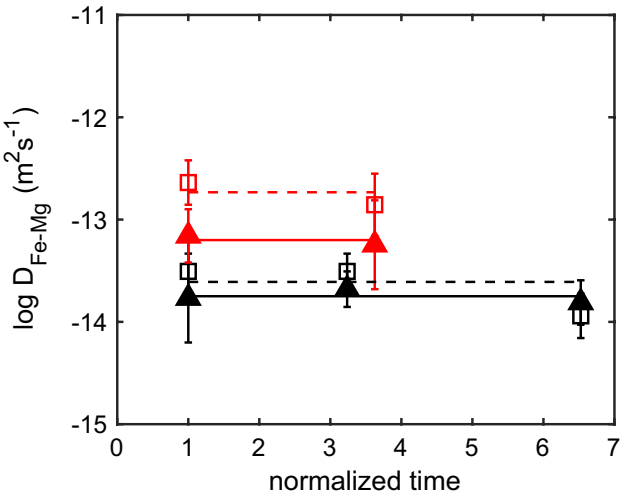


**Fig. 4** Diffusion coefficients determined from time series experiments at 1000 °C (black) and 1100 °C (red). The results are plotted against the run duration normalized to the duration of the shortest experiment in the time series. Open squares indicate the results from the geikielite single crystal. Closed triangles represent the results obtained from the ilmenite polycrystal. The plotted uncertainty is the 70% confidence interval reported in Table 2

1 day, respectively). Again, the results from the ilmenite and geikielite sides are within the estimated uncertainty for the two time points.

## Temperature dependence

The experimentally determined interdiffusion coefficients, $D_{Fe-Mg}$ or $D_{Fe-Mn}$, for each diffusion couple type have been fit separately to the Arrhenius equation:

$$\ln D = \ln D_0 - \frac{Q}{RT}, \quad (3)$$

where $D_0$ is the pre-exponential factor (m$^2$ s$^{-1}$), $Q$ is the activation energy (J mol$^{-1}$), $R$ is the universal gas constant (J mol$^{-1}$ K$^{-1}$) and $T$ is temperature (K). The activation energy and pre-exponential factor for each set of experiments was determined by linear regression (Table 3). The method of weighted least squares and the uncertainty on the average $D$ from each experiment (reported in Table 2) were used to estimate the uncertainty on the calculated activation energy and $D_0$ for each diffusion couple type (Table 3).

### Fe–Mg interdiffusion

The difference in the experimental design for the two sets of Fe–Mg interdiffusion experiments was the orientation of the geikielite crystal (with diffusion either perpendicular or parallel to the $c$-axis). For Fe–Mg interdiffusion experiments,

**Table 3** Experimentally determined Arrhenius fit parameters and uncertainties

| Type | $Q$ (kJ mol$^{-1}$) | log D$_0$ (m$^2$ s$^{-1}$) |
|---|---|---|
| **Fe–Mg** | | |
| Geikielite ⊥c | 224 ± 20 | − 4.5 ± 0.8 |
| Geikielite ‖c | 239 ± 39 | − 3.6 ± 1.7 |
| | **220 ± 16** | **− 4.6 ± 0.7** |
| Ilmenite | **188 ± 15** | **− 6.0 ± 0.6** |
| **Fe–Mn** | | |
| Ilmenite | 262 ± 30 | − 3.0 ± 1.2 |
| Mn-ilmenite | 241 ± 34 | − 3.6 ± 1.4 |
| | **264 ± 30** | **− 2.9 ± 1.3** |

Reported uncertainty (1$\sigma$) was calculated from a weighted linear regression of the values reported in Table 2. For Fe–Mg interdiffusion, the bold values represent the parameters calculated from a weighted linear regression through the data from both orientations. For Fe–Mn interdiffusion, the bold values represent the parameters determined from the weighted linear regression through data from both sides of the experiment. The bold values have been used to plot the solid lines in Figs. 5, 6, and 7

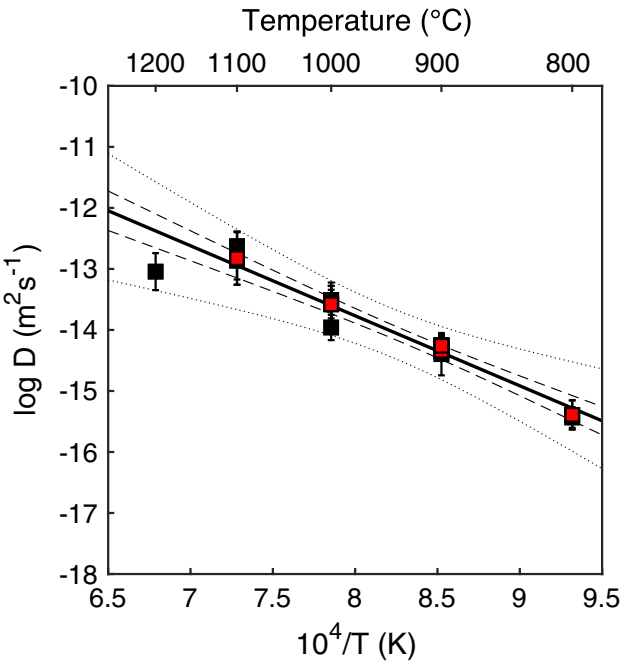


**Fig. 5** Arrhenius plot of results for Fe–Mg interdiffusion in the geikielite single crystal. Each square represents the average interdiffusion coefficient calculated for a given experiment, and the plotted uncertainty is the 70% confidence interval reported in Table 2. The black squares are for experiments where the geikielite was oriented such that diffusion occurred perpendicular to the $c$-axis (⊥c), and the red squares are for experiments where the geikielite was oriented such that diffusion occurred parallel to the $c$-axis (‖c). The solid line depicts the weighted linear regression through all points (both red and black), and the dashed lines show the uncertainty on this fit (70% confidence interval). The dotted lines depict the uncertainty on the linear fit at the 95% confidence interval

the results from the ilmenite polycrystal side of the diffusion couple are often the same as those from the geikielite single crystal within the estimated uncertainty (Table 2). The molar concentration of Ti in the geikielite (approximately 1.00–1.02 Ti cations per 3 oxygens) is slightly higher than that in the ilmenite (approximately 0.98–1.00 Ti cations per 3 oxygens). The Ti excess in the geikielite single crystal results from the method used to synthesize the crystal (Mitchell et al. 1998). Because the geikielite crystal has a higher Ti concentration than the ilmenite polycrystal and the diffusion coefficients might depend on Ti concentration, the two sides of the diffusion couple have been treated separately for the Arrhenius fits. Potential effects of Ti concentration on Fe–Mg interdiffusion are discussed in Sect. 4.3.

The results for Fe–Mg interdiffusion in the geikielite single crystal are similar for the two geikielite orientations, with $Q = 224 \pm 20$ kJ mol$^{-1}$ and $\log D_0 = -4.5 \pm 0.8$ m$^2$ s$^{-1}$ for diffusion perpendicular to the $c$-axis, and $Q = 239 \pm 39$ kJ mol$^{-1}$ and $\log D_0 = -3.6 \pm 1.7$ m$^2$ s$^{-1}$ for diffusion parallel to the $c$-axis. Thus, any crystallographic orientation effect on Fe–Mg interdiffusion in the geikielite single crystal was not evident in our results.

For Fe–Mg interdiffusion in the ilmenite polycrystal, we determined that $Q = 188 \pm 15$ kJ mol$^{-1}$ and $\log D_0 = -6.0 \pm 0.6$ m$^2$ s$^{-1}$. The reported averages and uncertainties were calculated using the diffusion profile fitting results from the ilmenite polycrystals in both sets of Fe–Mg interdiffusion experiments (⊥c and ‖ c). Though slight differences exist for the two orientations (Fig. 6), the calculated temperature dependence for each orientation was the same within uncertainty ($Q = 191 \pm 23$ kJ mol$^{-1}$ and $\log D_0 = -5.9 \pm 0.9$ m$^2$ s$^{-1}$ for experiments where the geikielite was oriented with diffusion perpendicular to the $c$-axis; $Q = 196 \pm 25$ kJ mol$^{-1}$ and $\log D_0 = -5.6 \pm 1.1$ m$^2$ s$^{-1}$ for experiments where the geikielite was oriented with diffusion parallel to the $c$-axis). Comparing the results for the temperature dependence of Fe–Mg interdiffusion calculated for ilmenite and geikielite, we find that there is a small yet resolvable difference, with the activation energy for diffusion in the ilmenite polycrystal being lower than that for the geikielite single crystals.

#### Fe–Mn interdiffusion

For Fe–Mn interdiffusion, our experimental results yield $Q = 264 \pm 30$ kJ mol$^{-1}$ and $\log D_0 = -2.9 \pm 1.3$ m$^2$ s$^{-1}$. The reported averages and uncertainties were calculated using the diffusion profile fitting results from both sides of the diffusion couple (ilmenite polycrystal and Mn-bearing ilmenite polycrystal). When treated separately, the results from each side are the same within uncertainty. Manganese is present at low concentrations in the Fe–Mn interdiffusion experiments, and thus behaves as a trace (not major) component.

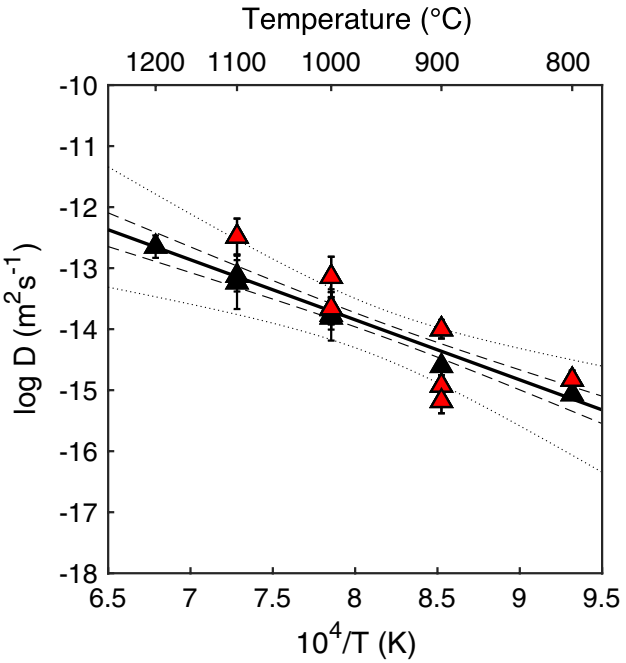


**Fig. 6** Arrhenius plot of results for Fe–Mg interdiffusion in the ilmenite polycrystal. Each triangle represents the average interdiffusion coefficient calculated for a given experiment, and the plotted uncertainty is the 70% confidence interval reported in Table 2. The black triangles are for experiments where the geikielite was oriented such that diffusion occurred perpendicular to the $c$-axis (⊥c), and the red triangles are for experiments where the geikielite was oriented such that diffusion occurred parallel to the $c$-axis (‖c). The solid line depicts the weighted linear regression through all points (both red and black), and the dashed lines show the uncertainty on this fit (70% confidence interval). The dotted lines depict the uncertainty on the linear fit at the 95% confidence interval

We did not find a Mn concentration dependence for Fe–Mn diffusion.

## Discussion

### Comparison to diffusion in hematite

One important distinction between ilmenite and hematite is the oxidation state of Fe, with all $Fe^{2+}$ in pure ilmenite and all $Fe^{3+}$ in pure hematite. Experimental studies of diffusion in hematite indicate that the diffusivity of Fe in hematite decreases with increasing oxygen fugacity ($f_{O_2}$) (Atkinson and Taylor 1985; Amami et al. 1999; Sabioni et al. 2005). This relationship between diffusion and $f_{O_2}$ suggests that Fe diffusion occurs by a diffusion mechanism involving interstitial sites, rather than a vacancy mechanism. Similar to the equation for cation vacancy formation in magnetite (Aggarwal and Dieckmann 2002), the formation of cation vacancies in ilmenite-hematite solid solution by oxidation of $Fe^{2+}$ to $Fe^{3+}$ can be written as

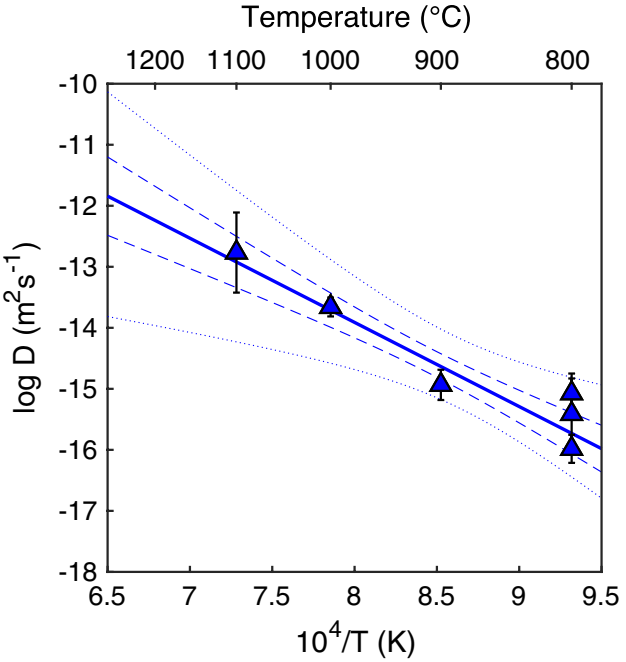


**Fig. 7** Arrhenius plot of results for Fe–Mn interdiffusion in the ilmenite and Mn-ilmenite polycrystals. Each triangle represents the average interdiffusion coefficient calculated from the ilmenite and Mn-bearing ilmenite polycrystals in a given experiment, and the plotted uncertainty is the 70% confidence interval reported in Table 2. The solid line depicts the weighted linear regressions through all points, and the dashed lines show the uncertainty on this fit (70% confidence interval). The dotted lines depict the uncertainty on the linear fit at the 95% confidence interval

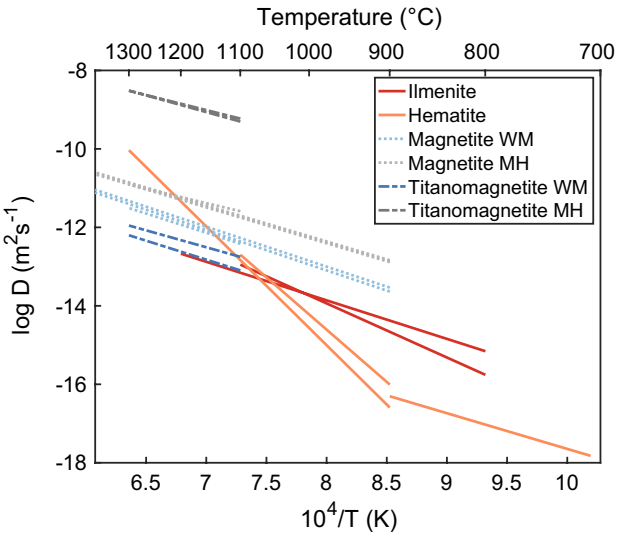


**Fig. 8** Comparison of results for diffusion in ilmenite, hematite, magnetite, and titanomagnetite. For ilmenite, one line represents the average of our reported results for Fe–Mg interdiffusion in ilmenite, and one line represents our reported results for Fe–Mn interdiffusion (bolded values in Table 3). For hematite, the Fe diffusivity parallel to the c-axis is plotted using values from Atkinson and Taylor (1985) and Sabioni et al. (2005). For magnetite, the lines represent the literature values for Fe and Mn diffusivity at the wüstite–magnetite (WM) and magnetite–hematite (MH) buffers from Dieckmann and Schmalzried (1977) and Aggarwal and Dieckmann (2002). For titanomagnetite ($X_{Ti} = 0.2$), the lines represent the literature values for Fe and Mn diffusivity at the wüstite–magnetite (WM) and magnetite–hematite (MH) buffers from Aggarwal and Dieckmann (2002)

$$3\,Fe^{2+} + \frac{3}{4}O_2 \longleftrightarrow 2\,Fe^{3+} + V_M + \frac{1}{2}Fe_2O_3,$$

where $V_M$ represents a vacant cation site. This reaction indicates that diffusion through cation vacancies would be faster at higher $f_{O_2}$ because oxygen promotes cation vacancy formation. However, previous studies have determined Fe diffusion in hematite to be slower at higher oxygen fugacities, which indicates that the diffusion of Fe in hematite occurs by cation interstitials rather than cation vacancies (see Sect. 4.3 for additional discussion of diffusion mechanisms).

The activation energies reported from experimental studies of Fe self-diffusion parallel to the *c*-axis in hematite single crystals range from 510 to 579 kJ mol$^{-1}$ for temperatures between 900 and 1300 °C (Sabioni et al. 2005; Amami et al. 1999; Atkinson and Taylor 1985). Atkinson and Taylor (1985) found that the activation energy for Fe diffusion in hematite was lower (174 kJ mol$^{-1}$) at temperatures below 900 °C and attributed this change to impurities or point defects, concluding that the high-temperature behavior was more characteristic of pure hematite. Sabioni et al. (2005) found that Fe diffusion in hematite varies as a function of crystallographic orientation, with diffusion perpendicular to the *c*-axis having an activation energy of 430 kJ mol$^{-1}$. Further, Sabioni et al. (2005) found that between 900 and 1100 °C diffusion perpendicular to the *c*-axis is slower than diffusion parallel to the *c*-axis in hematite. These activation energies are approximately double that of Fe–Mg interdiffusion in ilmenite (Sect. 3.2). Because of the difference in activation energies and $D_0$ for Fe diffusion in hematite and ilmenite, Fe diffusion will be faster in hematite above 1100 °C and faster in ilmenite below 1100 °C (Fig. 8).

## Comparison to diffusion in magnetite and titanomagnetite

Cation diffusivities in magnetite have been experimentally determined and characterized as a function of temperature, $f_{O_2}$ and composition (Van Orman and Crispin 2010, and references therein). At $f_{O_2}$ near the wüstite–magnetite (WM) buffer, Fe and Mn diffusion in magnetite occurs by a diffusion mechanism involving interstitial sites, similar to diffusion in hematite. In contrast, Fe and Mn diffusion in magnetite dominantly occurs via vacancies at $f_{O_2}$ near the magnetite–hematite buffer. Further, at reducing conditions, cation diffusion rates in magnetite are similar to that in

titanomagnetite; however, at more oxidizing conditions diffusion in titanomagnetite is faster than in magnetite because the presence of $Ti^{4+}$ promotes the formation of vacancies.

The activation energies for Fe diffusion in magnetite range from 148 to 230 kJ $mol^{-1}$ (Himmel et al. 1953; Izbekov 1958; Ogawa et al. 1968; Dieckmann and Schmalzried 1977; Aggarwal and Dieckmann 2002). Aggarwal and Dieckmann (2002) determined the activation energies for Mn and Ti diffusion in magnetite (Mn, 140–188 kJ $mol^{-1}$; Ti, 208–267 kJ $mol^{-1}$), as well as for Fe and Mn diffusion in titanomagnetite ($X_{Ti} = 0.2$; Fe, 147–165 kJ $mol^{-1}$; Mn, 163–185 kJ $mol^{-1}$). Our experimentally determined activation energy for Fe–Mg in the ilmenite polycrystal ($188 \pm 15$ kJ $mol^{-1}$) is within range of those reported for Fe and Mn diffusion in magnetite and titanomagnetite. The activation energy for Fe–Mg interdiffusion in ilmenite is also similar to that reported for Fe–Mg interdiffusion in synthetic spinel ($219 \pm 18$ kJ $mol^{-1}$ Vogt et al. 2015). Our reported activation energy for Fe–Mn interdiffusion in ilmenite ($264 \pm 30$ kJ $mol^{-1}$) is greater than the activation energies reported for Fe and Mn diffusion in magnetite and titanomagnetite, but similar to those reported for Ti diffusion in titanomagnetite. Additionally, the activation energies calculated for Fe–Mg interdiffusion in the geikielite single crystals ($224 \pm 20$ kJ $mol^{-1}$and $239 \pm 39$ kJ $mol^{-1}$) are within range of those reported for Ti diffusion in titanomagnetite.

Coexisting iron–titanium oxides are widely used to estimate pre-eruptive temperatures and oxygen fugacities in volcanic systems (Fish Canyon Tuff, Bishop Tuff, Soufrière Hills, Pinatubo, Mt. Unzen, Mt. St. Helens, Mt. Pelée, and many more). This geothermometer and oxybarometer is based on the exchange of Fe and Ti between coexisting rhombohedral oxide (ilmenite–hematite solid solution) and spinel (magnetite–ulvöspinel solid solution) phases. Our Fe–Mg and Fe–Mn interdiffusion coefficients were determined between 800 and 1100 °C, which overlaps the range of natural magmatic temperatures relevant to two-oxide equilibration (geothermometer initially calibrated between 600 and 1000 °C, Buddington and Lindsley 1964). Ghiorso and Evans (2008) found that for a database of 730 natural oxide pairs, the estimated oxygen fugacities relative to the nickel–nickel oxide buffer (NNO) fell within NNO ± 2. For temperatures 600–1000 °C this range corresponds to oxygen fugacities more oxidizing than the WM buffer. At oxygen fugacities above WM, diffusion of Fe and Mn in titanomagnetite is faster than Fe and Mn diffusion in ilmenite and this difference increases with $f_{O_2}$ (Fig. 8). At temperatures below 1000 °C, cation diffusion in ilmenite is faster than diffusion in hematite (Fig. 8). As $f_{O_2}$ increases, the ilmenite solid solution will become more enriched in the hematite component, and the diffusion rates will decrease. In this way, the cation diffusivities in hemo-ilmenite and titanomagnetite will "diverge" at lower temperature and higher $f_{O_2}$, and equilibration between the two oxides will be rate limited by diffusion in the rhombohedral oxide.

## Potential diffusion mechanisms for Fe, Mg, and Mn in ilmenite

Diffusive exchange of $Fe^{2+}$ and $Mg^{2+}$ or $Mn^{2+}$ cations in ilmenite occurs by a mechanism involving either cation interstitials or cation vacancies. Our experiments were not designed to elucidate the diffusion mechanism, and additional investigation over a range of oxygen fugacities and ilmenite compositions is needed to draw strong conclusions. However, here we briefly discuss potential reactions for the formation of cation interstitials and vacancies in ilmenite to provide insight into potential diffusion mechanisms and how diffusivity would vary with composition for each.

Similar to the equation for the formation of cation interstitial defects in hematite (Atkinson and Taylor 1985), the formation of cation interstitials in ilmenite may occur through the reaction:

$$Fe_{Fe}^{\times} + 3\ O_{O}^{\times} \longleftrightarrow Fe_{i}^{\bullet\bullet} + 2e' + \frac{3}{2}O_2,$$

where $Fe_{Fe}^{\times}$ denotes Fe residing in a cation site, and $Fe_{i}^{\bullet\bullet}$ represents an interstitial Fe with +2 charge balanced by two electrons ($e'$). Here, the interstitial is on the same side of the equation as $O_2$. Thus, as oxygen fugacity increases, the reaction goes to the left side and the concentration of cation interstitials decreases. Minor oxidation during two of our diffusion annealing experiments may have increased the amount of $Fe^{3+}$ in the ilmenite of those experiments and affected our diffusion results. For experiments F045 and F051, ilmenite analyses with low analytical totals, Ti cation totals < 1, and Fe cation totals > 1 result from a minor hematite component in the ilmenite (< 4 and < 2 mol% $Fe_2O_3$, respectively). At a given temperature, the calculated Fe–Mg interdiffusion coefficients are lower for experimental ilmenites that contained a minor hematite component (though still within our estimated uncertainty). Titanium-induced cation vacancies in the geikielite single crystal may explain why diffusion in the geikielite single crystals was faster than in the ilmenite polycrystal and why the results for both geikielite orientations were consistent. Excess Ti in ilmenite would promote the formation of cation vacancies by the reaction:

$$2\ M_{A}^{\times} + TiO_2 \longleftrightarrow Ti_{A}^{\bullet\bullet} + V_{A}'' + 2\ MO,$$

where $M$ in the equation denotes $Fe^{2+}$, $Mg^{2+}$, or $Mn^{2+}$ cations. Here, the excess $Ti^{4+}$ resides in $A^{2+}$ sites ($Ti_{A}^{\bullet\bullet}$), promoting A-site cation vacancies ($V_{A}''$) to maintain charge balance. In our diffusion annealing experiments the molar concentration of Ti in the geikielite (approximately 1.00–1.02 Ti cations per 3 oxygens) is higher than that in the ilmenite

(approximately 0.98–1.00 Ti cations per 3 oxygens). In many of the Fe–Mg experiments, there is slight zoning in Ti concentrations decreasing from the geikielite across the interface into the ilmenite, suggesting Ti may have diffused from the geikielite single crystal into the ilmenite polycrystal (Fig. 9). Diffusion involving Ti-induced cation vacancies may explain why the diffusion in the ilmenite polycrystal is slower than that in the geikielite crystal for these experiments. Titanium concentration profiles are not observed for any of the Fe–Mn interdiffusion experiments.

There is potential for grain boundary diffusion to enhance diffusion rates in the ilmenite polycrystal relative to the geikielite single crystal, but we did not observe evidence for this mechanism having a significant effect on our results. Although the ilmenite polycrystals from two experiments conducted at the same temperature (1000 °C, F019 and F045) exhibit different grain sizes (Online Resource 4), the calculated Fe–Mg interdiffusion coefficients are the same within uncertainty (Table 2). Additionally, there were no changes in concentration corresponding to the location of grain boundaries in the electron microprobe traverses on the ilmenite polycrystals from our experiments. Previous comparisons of single crystal and polycrystalline studies for Fe diffusion in hematite have similarly concluded that there is no contribution from rapid grain boundary diffusion (Atkinson and Taylor 1985).

Our experimental results cannot conclusively determine which mechanism is controlling the diffusion of cations in ilmenite; however, there are two important observations to consider: (1) the presence of $Fe^{3+}$ in two of the ilmenite polycrystals resulted in decreased diffusivity in the ilmenite compared to the geikielite, and (2) titanium excess in the geikielite single crystals can promote cation vacancy formation and may explain why diffusion in the geikielite is faster than that in the ilmenite.

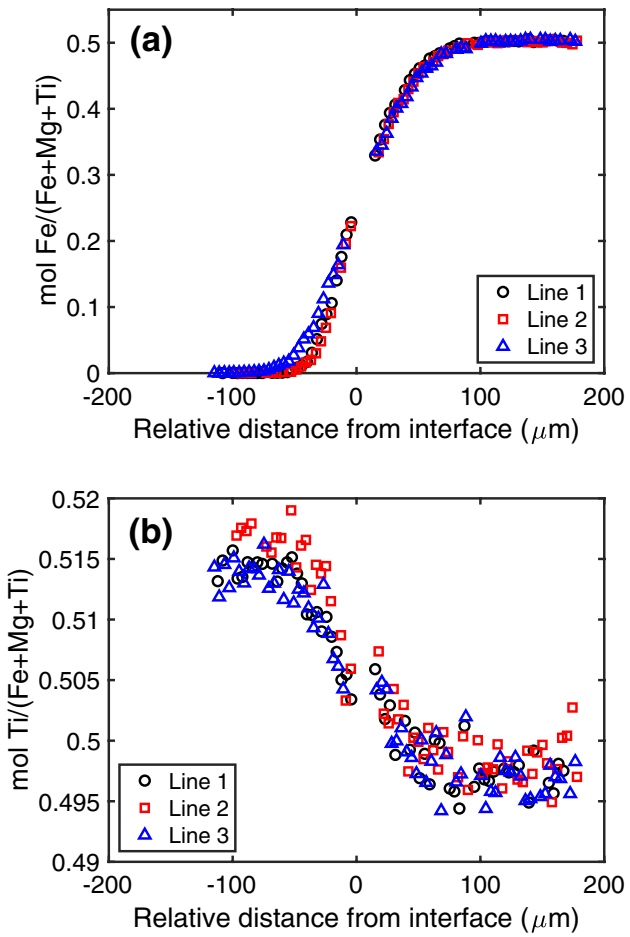


**Fig. 9** Electron microprobe analyses of experiment F032 plotted as a function of distance from the diffusion interface. **a** Three Fe concentration profiles for the diffusion couple. **b** The observed Ti concentration gradient for each analytical traverse in **a**, with greater Ti concentration in the geikielite side of the diffusion couple

## Applications

Moving forward we will apply our experimentally determined diffusion rates to natural ilmenite-bearing systems. Coupling our experimentally determined diffusion coefficients with preserved chemical disequilibria in natural ilmenites provides a mechanism by which to constrain the timing of perturbations in magmatic systems. For Fe–Mg interdiffusion we will use an activation energy of 188 kJ $mol^{-1}$ and $\log D_0$ of − 6.0 $m^2$ $s^{-1}$, which is the value obtained from the weighted linear regression through the diffusion results from the polycrystalline ilmenite side of our diffusion couple experiments (Table 3). We are using the Arrhenius curve from the ilmenite side of the diffusion couple because the composition of natural ilmenite crystals is more similar to the composition of the ilmenite polycrystal than the geikielite single crystal. For Fe–Mn interdiffusion, we will use the parameters determined by the weighted linear regression through data from both sides of the diffusion couple ($Q$ = 264 kJ $mol^{-1}$ and $\log D_0 = -2.9$ $m^2$ $s^{-1}$).

### Application to natural disequilibrium oxide pairs

Disequilibrium within an oxide crystal or between pairs is often interpreted to be a result of disturbances in the magmatic plumbing system such as injection of new magma, de-volatilization, and decompression (Gardner et al. 1995; Nakamura 1995; Pallister et al. 1996; Venezky and Rutherford 1999; Devine et al. 2003; Blundy et al. 2006; Pallister et al. 2008). These perturbations are potential precursors to eruptions or changes in eruption style, and thus are important to recognize and understand

(Wark et al. 2007; Bachmann and Bergantz 2008; Cashman and Sparks 2013).

A test for oxide pair equilibria was developed by Bacon and Hirschmann (1988) from the magnesium and manganese compositions of natural oxide pairs (hemo-ilmenite and titanomagnetite). Natural oxide pair compositions that fall off of this equilibrium line are often not reported. However, they have been found in many eruptive centers, including but not limited to Mt. St. Helens, Mt. Unzen, the Bishop Tuff, and the Fish Canyon Tuff (Ghiorso and Evans 2008). Titanium zoning in natural hemo-ilmenites and titanomagnetites provides additional evidence for oxide disequilibrium in volcanic samples from Mt. Unzen, Mt. St. Helens, Mt. Pinatubo, and Soufrière Hills (Gardner et al. 1995; Nakamura 1995; Pallister et al. 1996; Venezky and Rutherford 1999; Devine et al. 2003; Pallister et al. 2008; Rutherford and Devine III 2008). In practice, oxide pair compositions that do not fall on the empirical line defined by Bacon and Hirschmann (1988) are not used for geothermometry and oxybarometry. However, this oxide pair disequilibrium can instead place constraints on the conditions and timescales of volcanic processes, provided the diffusivities of Mg and Mn are known for both magnetite and ilmenite.

To preserve disequilibria in oxides, the time between perturbation and volcanic eruption must be shorter than the rate of mineral equilibration via diffusion. Silicate minerals preserve compositional evidence for temperature perturbations in a magmatic system on time scales that range from months to millions of years (Costa et al. 2008, and references therein). Cation diffusion in Fe–Ti oxides is faster than in silicate minerals, and compositional zoning will be diffusively equilibrated on short time scales (hours to months). Thus, oxide disequilibria record instances where the time between a thermal pulse and eruption is short. Determining the timescales of oxide equilibration can constrain the time between these two events.

Using our experimentally determined Fe–Mn interdiffusivities for ilmenite, we can model the time- and temperature-dependent equilibration of an ilmenite grain as a function of grain size. Approximating that the ilmenite grains are spherical, the time it would take an ilmenite grain of a given diameter to equilibrate after a heating or mixing event can be estimated using the following equation from McDougall et al. (1999):

$$f \approx 1 - 6/\pi^2 \exp((-\pi^2 Dt)/r^2), \quad (4)$$

where $f$ is the fractional approach to equilibrium, $D$ diffusion coefficient taken at a given temperature ($m^2\ s^{-1}$), $r$ grain radius (m), and $t$ the time (s) since the perturbation. This equation is an approximation that applies when $f >\sim 0.85$. In our modeling, we use $f = 0.95$ as the approximation for complete equilibration because this is within the uncertainty of the Mg/Mn filter.

Disequilibrium between oxide pairs has been observed for each of the volcanic centers discussed below (Johnson and Rutherford 1989; Venezky and Rutherford 1999; Rutherford and Devine III 2008; Bacon and Hirschmann 1988; Hildreth 1979; Whitney and Stormer Jr. 1985; Ghiorso and Evans 2008; Blundy et al. 2006; Pallister et al. 2008). Our experimental data characterize the interdiffusion of $Fe^{2+}$ and $Mn^{2+}$; however, $Fe^{3+}$ is present in natural volcanic systems. Given a significant $Fe_2O_3$ component, the ilmenite equilibration rates would likely be slower than those estimated in our calculations.

The reported ilmenite grain sizes for both the Bishop Tuff and the Fish Canyon Tuff range from 100 to 500 µm (Hildreth 1979; Whitney and Stormer Jr. 1985). The temperature range used for the Bishop Tuff calculation (700–790 °C, Hildreth and Wilson 2007) was estimated using equilibrated Fe–Ti oxide thermometry. The temperature range used for the Fish Canyon Tuff (730–790 °C, Johnson and Rutherford 1989) is the pre-eruptive temperature range deduced from experimental phase equilibrium data. For the Bishop Tuff and Fish Canyon Tuff the reported ilmenite grain sizes and estimated pre-eruptive temperatures suggest the time between thermal perturbation and eruption is on the order of months to decades (Fig. 10).

For Mt. Unzen, a pre-eruptive temperature range of 850–930 °C and ilmenite grain size range of 50–350 $\mu$m was used for the calculation (Venezky and Rutherford 1999).

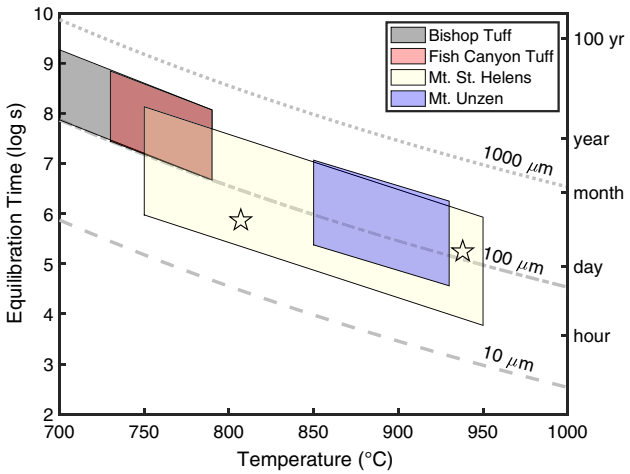


**Fig. 10** Equilibration times for ilmenite grains of a given size, calculated using our results for Fe–Mn interdiffusivity in ilmenite. The dashed lines indicate the time for a grain of a given diameter to equilibrate with respect to Fe and Mn as a function of temperature. The shaded regions were calculated using the characteristic grain sizes and pre-eruptive temperatures for the four volcanic complexes listed. The two stars represent the equilibration times calculated for two zoned ilmenite grains from Pallister et al. (2008)

This temperature range was estimated from a combination of Fe–Ti oxide thermometry and the results of phase equilibrium experiments. For Mt. St. Helens, a temperature range of 750–950 °C and grain size range of 25–300 $\mu$m was used in the calculation. These values encompass the temperature ranges estimated from Fe–Ti oxide thermometry for the 1980–1986 and 2004–2006 eruptions and the observed oxide grain sizes (Blundy et al. 2008; Pallister et al. 2008; Rutherford and Devine III 2008).

For ilmenite grains in volcanic samples from Mt. Unzen and Mt. St. Helens, the results of this calculation indicate that ilmenite equilibration times are on the order of hours to months (Fig. 10). Previously, compositional zoning of Ti in titanomagnetite has been used to estimate the time between thermal perturbation and eruption at Mt. Unzen (e.g., Nakamura 1995; Venezky and Rutherford 1999). These studies indicate that the 1991–1993 Mount Unzen eruption involved continuous replenishment of a dacitic magma source weeks (Venezky and Rutherford 1999) or months (Nakamura 1995) before eruption. At Mt. St. Helens, the pre-eruptive magma-mixing time for the 2004–2006 eruption is estimated to be less than 5–8 weeks from Ti compositional profiles preserved in titanomagnetite (Rutherford and Devine III 2008). Additionally for Mt. St. Helens, an ascent time of 2.6 weeks to 2.5 months has been estimated from the 2004–2006 magma eruption rates (Pallister et al. 2008), whereas an ascent time of 4–8 days has been estimated from the extent of groundmass crystallization in the 1980–1986 eruption products (Geschwind and Rutherford 1995). Our results are consistent with the previous estimates for the timing of magmatic activity at both volcanoes, and indicate that ilmenite zoning can record processes that occur in hours to months.

Constraints on the pre-eruptive temperature and grain size of zoned ilmenites lowers the uncertainty in the range of estimated equilibration times (Fig. 10). Given the wide range of temperatures estimated from Fe–Ti oxide thermometry for Mt. St. Helens, it is helpful to focus on specific observations of zoning in ilmenite to provide narrow time constraints on a given sample. For example, we have calculated the time it would take to equilibrate two zoned ilmenites reported in Pallister et al. (2008) (results plotted as stars in Fig. 10). For a zoned ilmenite from the 1980–1986 eruptive products (sample MSH05JV_1_19 in Pallister et al. 2008) with a reported grain size of 120 µm, the grain would equilibrate within 2 days at the reported temperature of 938 °C. This result indicates that the cause of chemical zoning occurred less than 2 days prior to eruption. Similarly, the 50 µm zoned ilmenite observed in a sample from the April 1 2005 eruption (sample SH315-2 in Pallister et al. 2008) would equilibrate within 8.5 days at the reported temperature of 807 °C, indicating the zoning formed less than 8.5 days before eruption. While the characteristic equilibration times in Fig. 10 provide useful time constraints for the volcanic activity at each volcano, these two examples illustrate the utility of our diffusion data when integrated with discrete observations of zoned ilmenites in natural samples.

## Application to magnesium zoning in kimberlite megacrysts

Kimberlites are volatile-rich, ultramafic, igneous rocks that contain diamonds and mantle xenoliths. Preservation of diamond through deep magma transport to the surface and ascent of dense mantle xenoliths both require rapid ascent rates. Magma ascent rates for kimberlites have been estimated to reach 30 m $s^{-1}$, which overwhelmingly exceeds the 5 m $s^{-1}$ estimate for other xenolith-bearing magmas (Rutherford 2008). Though kimberlites have been extensively studied, uncertainties still exist regarding kimberlite properties such as source composition, depth, temperature, and oxidation state (e.g., Mitchell 1995; Sparks 2013, and references therein).

Kimberlites may contain large (up to 20 cm) megacrysts of garnet, diopside, and ilmenite, referred to as the "megacryst suite". The origin of the megacryst suite has been widely debated; leading theories propose that the megacrysts crystallized at depths of 150–200 km from a magma that is either proto-kimberlitic or basaltic (Mitchell 1995). There have been many studies on the occurrence, mineralogy, and chemistry of the megacryst suite, particularly with aim to establish the megacryst minerals as an indicator for diamond-bearing kimberlites. However, the timing of megacryst incorporation into the kimberlite magma (i.e., prior to or during ascent) remains unconstrained.

Rapid kimberlite eruption preserves disequilibria between megacrysts and their kimberlitic host matrix in the form of compositional zoning and reaction rims. This disequilibrium is evidence of a perturbation to the megacryst source prior to eruption. Applying diffusion data to the observed disequilibria can help to constrain the timing of this perturbation and address whether the megacrysts are incorporated near the source of the kimberlite magma or during ascent.

The megacryst ilmenites found in kimberlites have characteristically high MgO contents (5–23 wt%) and low ferric iron abundances (0.2–20 wt% $Fe_2O_3$), making these samples ideal for demonstrating the utility of our $Fe^{2+}$-$Mg^{2+}$ interdiffusion rates for ilmenite. Additionally, there is widespread evidence for chemical diffusion in the ilmenites of the megacryst suite. One example of this is the preservation of Mg enrichment at the rims of ilmenite grains, yielding diffusion profiles that are on average 100–500 µm in length (Mitchell 1986). This Mg enrichment at the ilmenite rims results from incomplete equilibration between the ilmenite megacrysts and the Mg-rich kimberlitic host magma (Pasteris 1981).

Considering the megacryst suite as an isolated unit that is then sampled by kimberlite magma and brought to the surface, we can use our experimentally determined Fe–Mg interdiffusion rates for ilmenite to determine the timing of megacryst suite incorporation as it relates to kimberlite magma ascent. Specifically, this calculation estimates the duration of Fe–Mg exchange between the ilmenite and kimberlite using the equation

$$t = \frac{x^2}{D_{\mathrm{Fe-Mg}}} \tag{5}$$

where $t$ is time (s), $D_{\mathrm{Fe-Mg}}$ is the rate of Fe–Mg interdiffusion calculated as a function of temperature using our experimental results ($m^2\ s^{-1}$), and $x$ is the characteristic length of Mg diffusion into the ilmenite (m). For a given ilmenite megacryst, this $x$ corresponds to the distance from the rim at which the Mg concentration in the ilmenite equals the average of the core and rim Mg concentrations. The calculated durations, $t$, are compared to the estimated kimberlite ascent rates to establish whether the ilmenites were entrained by the kimberlite magma during ascent or whether the diffusive exchange between the kimberlite magma and megacryst ilmenites began prior to eruption.

Using our experimentally determined Fe–Mg interdiffusion rates for ilmenite, we have calculated the time it would take to develop a Mg diffusion profile of a given length in an ilmenite rim (Fig. 11). Our results from this calculation indicate that the Mg enrichment of ilmenite megacrysts would require ilmenite and kimberlitic magma to be in contact a minimum of hours to weeks depending on the exact temperature. The plotted range of temperatures in Fig. 11 encompasses both the estimated kimberlite source temperatures (1350–1450 °C, Priestley and McKenzie 2006; Sparks 2013), crystallization temperatures calculated from olivine-spinel geothermometry (1030–1170 °C, Fedortchouk and Canil 2004), and temperature estimates from models for the ascending magma which consider cooling upon ascent, volatile content, xenolith assimilation, and olivine crystallization (1050–1450 °C from source to eruption, Kavanagh and Sparks 2009).

To provide context for the $\sqrt{Dt}$ distances from the rim in Fig. 11, we have applied our Fe–Mg interdiffusion results to a core-to-rim profile of Mg enrichment measured in a natural kimberlitic ilmenite megacryst by Boctor and Boyd (1980) (Fig. 12). Using equation 2, we linearized the observed profile, then determined the slope, $(4Dt)^{-1/2}$, from a linear regression through the analytical points. With this slope and our experimentally determined temperature dependence for $D_{\mathrm{Fe\text{-}Mg}}$, we calculated the time for the observed Mg-enrichment profile to form by diffusion as a function of temperature (Fig. 11). The modeled Mg-enrichment profile has been plotted as an error function in Fig. 12 using Eq. 1.

Consider that the ilmenite megacrysts are sampled from a source depth of 150 km. For magma temperatures greater than 1300 °C, 100 µm rims of Mg enrichment form within hours, suggesting the interaction could take place solely

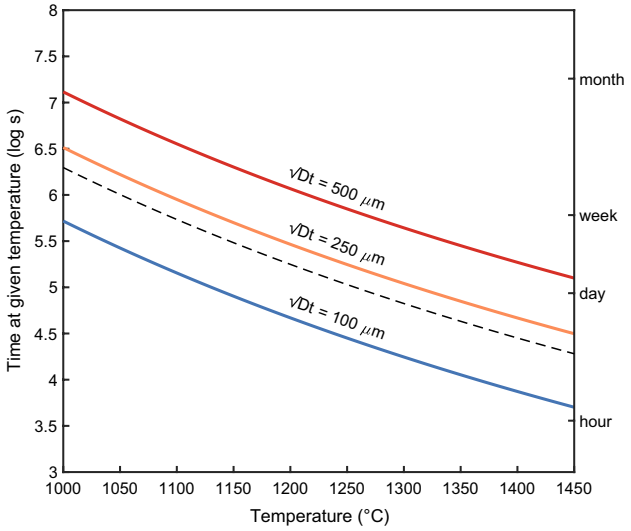


**Fig. 11** Calculated times for Mg-enrichment rims to form by Fe–Mg interdiffusion. Each solid line represents a given length of Mg enrichment at the rim of an ilmenite grain, and indicates the time it would take that enrichment profile to form at a given temperature. The temperature range of the $x$-axis encompasses the range of estimates for the source temperatures of the host kimberlite magma (Sect. 5.2). The dashed line represents the results calculated from a core-to-rim profile of Mg enrichment measured in a natural ilmenite megacryst by Boctor and Boyd (1980) (Fig. 12)

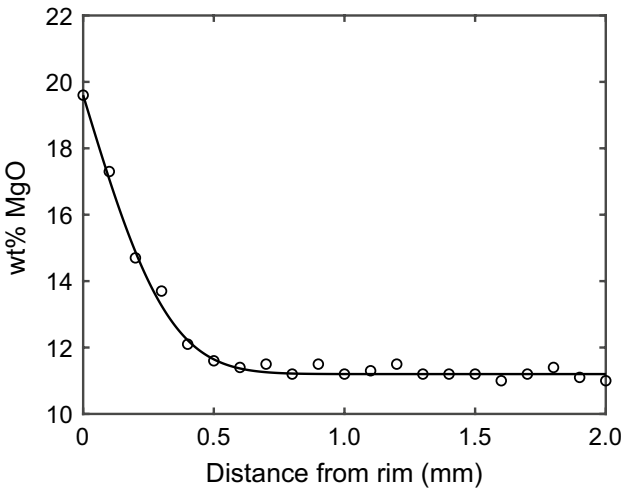


**Fig. 12** Magnesium enrichment profile observed in a natural kimberlitic ilmenite megacryst. The open circles represent the electron microprobe analyses reported in Boctor and Boyd (1980). The solid line depicts our modeled error function fit for the measured profile. The modeled profile was used to calculate the time needed to form the observed Mg-enrichment rim at a given temperature (Fig. 11)

during the rapid ascent stage of kimberlite eruption (10–30 m $s^{-1}$). However at these temperatures, the 500 µm rims of Mg enrichment would still require at least a day of interaction with the kimberlite magma. If this interaction occurred only during the ascent stage, this time would roughly translate to kimberlite ascent rates < 2 m $s^{-1}$, which is an order of magnitude slower than previous estimates. This result indicates that either the initial stage of kimberlite magmatic ascent is slow enough to allow for days to weeks of interaction between the kimberlite and megacrysts, or alternatively, that the kimberlite magma and megacrysts are interacting prior to the onset of eruptive ascent.

The initial stage of ascent for xenolith carrying magmas constitutes a majority of the ascent time, and the ascent rates for this stage have been estimated to be between 2.9 and 16.8 m $s^{-1}$ (Rutherford 2008). If the initial ascent of the kimberlite magma occurs at a rate of 3 m $s^{-1}$, then the ascent time from 150 km would be approximately 14 h. From our diffusion results, we have determined that an interaction time of 14 h could produce 100–500 µm rims of Mg enrichment in an ilmenite grain given a temperature range of 1200–1600 °C. If the 2.9 m $s^{-1}$ ascent rate is relevant to the initial stages of kimberlite ascent, then the temperature of the kimberlite host magma can be approximated using the width of the Mg-enrichment rims on the ilmenite megacrysts.

The growth of spinel rims on garnets has previously been used in a similar way to decipher the timing of garnet incorporation into kimberlite magma (Canil and Fedortchouk 1999). However, the reported timescales required to form approximately 25 µm spinel rims on garnet at temperatures between 1000 and 1200 °C are on the order of hours, and at 1400 °C would form within minutes. These timescales indicate that the kelyphitic rims form at either at lower temperatures or shorter timescales than those for the diffusion of Mg into ilmenite megacrysts.

Our experimentally determined cation interdiffusion rates for ilmenite provide a new geospeedometry tool that, when applied to the disequilibrium preserved in kimberlite ilmenite megacrysts, elucidates the processes related to kimberlite magma storage and incorporation of the megacryst suite. It is important to note that in calculating the times to form the observed Mg enrichment at the rims of ilmenite megacrysts we have made consistent assumptions that would result in minimum estimates. All calculations were performed assuming all Fe was present as $Fe^{2+}$, though in reality $Fe^{3+}$ is present and thus the Fe–Mg interdiffusion rates would be slower. Additionally, grain boundary erosion occurs during ascent and would decrease the profile length (and thus time estimate). Lastly, the formation of perovskite reaction rims on ilmenite megacrysts might also hinder the diffusion of Mg into the ilmenite megacryst. Given these assumptions, it is most likely that the megacryst suite is chemically interacting with the kimberlitic magma prior to the onset of eruptive ascent. This argues for the megacryst suite being present in or near the source region of kimberlitic magmas, rather than being incorporated during ascent like peridotite xenoliths.

## Conclusions

From our experimentally determined Fe–Mg and Fe–Mn interdiffusivities, we find that diffusion in ilmenite is faster than in hematite. Our results indicate that crystallographic orientation did not affect diffusion rates in ilmenite. To apply this data to natural systems, for Fe–Mg interdiffusion we use an activation energy ($Q$) of 188 kJ $mol^{-1}$ and $\log D_0$ of − 6.0 $m^2$ $s^{-1}$, and for Fe–Mn interdiffusion we use $Q$ = 264 kJ $mol^{-1}$ and $\log D_0 = -2.9$ $m^2$ $s^{-1}$. Because diffusion in ilmenite is slower than in magnetite, the diffusive exchange between rhombohedral oxide and spinel pairs used in geothermometers and oxybarometers will likely be rate-limited by diffusion in ilmenite–hematite solid solutions. In applying our data to disequilibrium observed in ilmenites from natural volcanic samples, we have estimated the time between perturbation and eruption for the Bishop Tuff, Fish Canyon Tuff, Mt. Unzen, Mt. St. Helens, and kimberlites. In this way, our experimentally determined diffusivities for ilmenite have provided a new tool with which to estimate the timing of volcanic activity.

**Acknowledgements** The authors would like to thank Paul Carpenter for his assistance with and discussions regarding electron microprobe analysis, Dr. Noah McLean for his suggestion of statistical approaches to apply our data, as well as Dr. Jill Pasteris for sharing her expertise in kimberlite megacrysts. Additionally, the authors thank two anonymous reviewers for providing thoughtful comments on this manuscript, and Dr. Mark Ghiorso for editorial handling. This work was supported by the Roger B. Chaffee fellowship from the McDonnell Center for the Space Sciences and NASA Earth and Space Sciences Fellowship Grant number 80NSSC17K0476 to KBP, and NSF Petrology and Geochemistry Grant EAR1654683 to MJK.

## References

Aggarwal S, Dieckmann R (2002) Point defects and cation tracer diffusion in $(Ti_xFe_{(1-x)})_{3-\delta}O_4$ 1. Non-stoichiometry and point defects. Phys Chem Miner 29(10):695–706

Amami B, Addou M, Millot F, Sabioni A, Monty C (1999) Self-diffusion in $\alpha$-$Fe_2O_3$ natural single crystals. Ionics 5(5–6):358–370

Atkinson A, Taylor R (1985) Diffusion of $^{55}Fe$ in $Fe_2O_3$ single crystals. J Phys Chem Solids 46(4):469–475

Bachmann O, Bergantz G (2008) The magma reservoirs that feed supereruptions. Elements 4(1):17–21

Bacon CR, Hirschmann MM (1988) Mg/Mn partitioning as a test for equilibrium between coexisting Fe–Ti oxides. Am Mineral 73(1–2):57–61

Bishop FC (1980) The distribution of $Fe^{2+}$ and Mg between coexisting ilmenite and pyroxene with applications to geothermometry. Am J Sci 280(1):46–77

Blundy J, Cashman K, Humphreys M (2006) Magma heating by decompression-driven crystallization beneath andesite volcanoes. Nature 443(7107):76

Blundy J, Cashman KV, Berlo K (2008) Evolving magma storage conditions beneath Mount St. Helens inferred from chemical variations in melt inclusions from the 1980–1986 and current (2004–2006) eruptions: chapter 33 in A volcano rekindled: the renewed eruption of Mount St. Helens, 2004-2006. Tech. rep., US Geological Survey

Boctor NZ, Boyd F (1980) Oxide minerals in the Liqhobong kimberlite. Lesotho. Am Mineral 65(7–8):631–638

Boyd F, England J (1960) Apparatus for phase-equilibrium measurements at pressures up to 50 kilobars and temperatures up to 1750°C. J Geophys Res 65(2):741–748

Buddington A, Lindsley D (1964) Iron-titanium oxide minerals and synthetic equivalents. J Petrol 5(2):310–357

Canil D, Fedortchouk Y (1999) Garnet dissolution and the emplacement of kimberlites. Earth Planet Sci Lett 167(3–4):227–237

Cashman KV, Sparks RSJ (2013) How volcanoes work: a 25 year perspective. GSA Bull 125(5–6):664–690

Chakraborty S (1997) Rates and mechanisms of Fe–Mg interdiffusion in olivine at 980°-1300°C. J Geophys Res Solid Earth 102(B6):12317–12331

Costa F, Dohmen R, Chakraborty S (2008) Time scales of magmatic processes from modeling the zoning patterns of crystals. Rev Mineral Geochem 69(1):545–594

Crank J (1975) The mathematics of diffusion, second, edition edn. Oxford University Press, Oxford

Devine J, Rutherford M, Norton G, Young S (2003) Magma storage region processes inferred from geochemistry of Fe–Ti oxides in andesitic magma, Soufriere Hills Volcano, Montserrat. WI. J Petrol 44(8):1375–1400

Dieckmann R, Schmalzried H (1977) Defects and cation diffusion in magnetite (i). Berichte der Bunsengesellschaft für physikalische Chemie 81(3):344–347

Fedortchouk Y, Canil D (2004) Intensive variables in kimberlite magmas, Lac de Gras, Canada and implications for diamond survival. J Petrol 45(9):1725–1745

Gardner JE, Carey S, Rutherford MJ, Sigurdsson H (1995) Petrologic diversity in Mount St. Helens dacites during the last 4,000 years: implications for magma mixing. Contrib Mineral Petrol 119(2–3):224–238

Geschwind CH, Rutherford MJ (1995) Crystallization of microlites during magma ascent: the fluid mechanics of 1980–1986 eruptions at Mount St Helens. Bull Volcanol 57(5):356–370

Ghiorso MS, Evans BW (2008) Thermodynamics of rhombohedral oxide solid solutions and a revision of the Fe–Ti two-oxide geothermometer and oxygen-barometer. Am J Sci 308(9):957–1039

Hildreth W (1979) The Bishop Tuff: evidence for the origin of compositional zonation in silicic magma chambers. Geol Soc Am Special Paper 180:43–75

Hildreth W, Wilson CJ (2007) Compositional zoning of the Bishop Tuff. J Petrol 48(5):951–999

Himmel L, Mehl R, Birchenall CE (1953) Self-diffusion of iron in iron oxides and the Wagner theory of oxidation. JOM 5(6):827–843

Izbekov V (1958) Diffusion of Fe in magnetite. Inzh-Fiz Zh 1:64–68

Johannes W, Bell P, Mao H, Boettcher A, Chipman D, Hays J, Newton R, Seifert F (1971) An interlaboratory comparison of piston-cylinder pressure calibration using the albite-breakdown reaction. Contrib Mineral Petrol 32(1):24–38

Johnson MC, Rutherford MJ (1989) Experimental calibration of the aluminum-in-hornblende geobarometer with application to Long Valley caldera (California) volcanic rocks. Geology 17(9):837–841

Kavanagh JL, Sparks RSJ (2009) Temperature changes in ascending kimberlite magma. Earth Planet Sci Lett 286(3–4):404–413

McDougall I, Mac Dougall I, Harrison TM et al (1999) Geochronology and thermochronology by the $^{40}Ar/^{39}Ar$ method. Oxford University Press, Oxford

Médard E, McCammon CA, Barr JA, Grove TL (2008) Oxygen fugacity, temperature reproducibility, and $H_2O$ contents of nominally anhydrous piston-cylinder experiments using graphite capsules. Am Mineral 93(11–12):1838–1844

Mitchell JN, Yu N, Sickafus KE, Nastasi MA, McClellan KJ (1998) Ion irradiation damage in geikielite ($MgTiO_3$). Philos Mag A 78(3):713–725

Mitchell RH (1986) Kimberlites: mineralogy, geochemistry, and petrology. Springer Science & Business Media, New York

Mitchell RH (1995) Kimberlites, orangeites, and related rocks. Springer Science & Business Media, New York

Müller T, Dohmen R, Becker H, Ter Heege JH, Chakraborty S (2013) Fe–Mg interdiffusion rates in clinopyroxene: experimental data and implications for Fe–Mg exchange geothermometers. Contrib Mineral Petrol 166(6):1563–1576

Nakamura M (1995) Continuous mixing of crystal mush and replenished magma in the ongoing Unzen eruption. Geology 23(9):807–810

Ogawa S, Nakajima T, Sasaki T, Takahashi M (1968) Ion diffusion and disaccommodation in ferrites. Jpn J Appl Phys 7(8):899

Pallister JS, Hoblitt RP, Meeker GP, Knight RJ, Siems DF (1996) Magma mixing at Mount Pinatubo: petrographic and chemical evidence from the 1991 deposits. Fire and mud: eruptions and lahars of Mount Pinatubo, Philippines pp 687–731

Pallister JS, Thornber CR, Cashman KV, Clynne MA, Lowers H, Mandeville CW, Brownfield IK, Meeker GP (2008) Petrology of the 2004-2006 Mount St. Helens lava dome–implications for magmatic plumbing and eruption triggering: Chapter 30 in A volcano rekindled: the renewed eruption of Mount St. Helens, 2004-2006. Tech. rep., US Geological Survey

Pasteris JD (1981) The significance of groundmass ilmenite and megacryst ilmenite in kimberlites. Contrib Mineral Petrol 75(4):315–325

Pownceby MI, Wall VJ, O'Neill HSC (1987) Fe-Mn partitioning between garnet and ilmenite: experimental calibration and applications. Contrib Mineral Petrol 97(1):116–126

Priestley K, McKenzie D (2006) The thermal structure of the lithosphere from shear wave velocities. Earth Planet Sci Lett 244(1–2):285–301

Rutherford MJ (2008) Magma ascent rates. Rev Mineral Geochem 69(1):241–271

Rutherford MJ, Devine III JD (2008) Magmatic conditions and processes in the storage zone of the 2004-2006 Mount St. Helens dacite: Chapter 31 in A volcano rekindled: the renewed eruption of Mount St. Helens, 2004–2006. Tech. rep., US Geological Survey

Sabioni A, Huntz AM, Daniel A, Macedo W (2005) Measurement of iron self-diffusion in hematite single crystals by secondary ion-mass spectrometry (SIMS) and comparison with cation self-diffusion in corundum-structure oxides. Philos Mag 85(31):3643–3658

Schulze DJ, Anderson PF, Hearn BC Jr, Hetman CM (1995) Origin and significance of ilmenite megacrysts and macrocrysts from kimberlite. Int Geol Rev 37(9):780–812

Shea T, Costa F, Krimer D, Hammer JE (2015) Accuracy of timescales retrieved from diffusion modeling in olivine: a 3D perspective. Am Mineral 100(10):2026–2042

Sparks R (2013) Kimberlite volcanism. Annu Rev Earth Planet Sci 41:497–528

Taylor LA, Uhlmann D, Hopper R, Misra K (1975) Absolute cooling rates of lunar rocks-theory and application. Lunar Planet Sci Conf Proc 6:181–191

Till CB, Vazquez JA, Boyce JW (2015) Months between rejuvenation and volcanic eruption at Yellowstone caldera. Wyoming. Geology 43(8):695–698

Ulmer P, Luth RW (1991) The graphite-COH fluid equilibrium in P, T, $f_{O_2}$ space. Contrib Mineral Petrol 106(3):265–272

Van Orman JA, Crispin KL (2010) Diffusion in oxides. Rev Mineral Geochem 72(1):757–825

Venezky DY, Rutherford MJ (1999) Petrology and Fe–Ti oxide reequilibration of the 1991 Mount Unzen mixed magma. J Volcanol Geotherm Res 89(1–4):213–230

Vogt K, Dohmen R, Chakraborty S (2015) Fe–Mg diffusion in spinel: new experimental data and a point defect model. Am Mineral 100(10):2112–2122

Wark D, Hildreth W, Spear F, Cherniak D, Watson E (2007) Pre-eruption recharge of the Bishop magma system. Geology 35(3):235–238

Watson E, Wark D, Price J, Van Orman J (2002) Mapping the thermal structure of solid-media pressure assemblies. Contrib Mineral Petrol 142(6):640–652

Whitney JA, Stormer JC Jr (1985) Mineralogy, petrology, and magmatic conditions from the Fish Canyon Tuff, central San Juan volcanic field. Colorado. J Petrol 26(3):726–762

Zhang Y, Cherniak DJ (2010) Diffusion in minerals and melts. Rev Mineral Geochem 72(1):603–756